NANO LETTERS

2006
Vol. 6, No. 11
2622−2625

Polarization-Selective Plasmon-Enhanced Silicon Quantum-Dot Luminescence

Hans Mertens,*,† Julie S. Biteen,‡ Harry A. Atwater,‡ and Albert Polman†

Center for Nanophotonics, FOM Institute for Atomic and Molecular Physics, Kruislaan 407, 1098 SJ Amsterdam, The Netherlands, and California Institute of Technology, 1200 East California Boulevard, Pasadena, California 91125

Received June 28, 2006; Revised Manuscript Received September 28, 2006

ABSTRACT

The photoluminescence intensity of silicon quantum dots is enhanced in a polarization-selective way by coupling to elongated Ag nanoparticles. The observed polarization dependence provides direct proof that the PL enhancement is due to electromagnetic coupling of the silicon quantum-dot emission dipoles with dipolar plasmon modes of the Ag nanoparticles. The polarization selectivity demonstrates the potential of engineered plasmonic nanostructures to optimize and tune the performance of light sources in a way that goes beyond solely enhancing the emission and absorption rates.

In recent years, the control of spontaneous emission by metallic nanostructures has regained considerable interest following up on the pioneering work that was performed in conjunction with studies on surface-enhanced Raman scattering (SERS) in the 1970s and 1980s.[1] These early investigations, which focused on the interaction of emitters with rough metal surfaces, resulted in the observation of surface-enhanced fluorescence (SEF).[2] In addition, semiclassical models were developed that describe SEF based on the electromagnetic coupling of dipole emitters with plasmon modes, that is, collective conduction electron oscillations, in metal nanoparticles.[3,4] These models predict large modifications of the excitation rate as well as of the radiative and nonradiative decay rates upon coupling emitters to metallic nanostructures.

The renewed interest in plasmon-enhanced fluorescence during the past decade was motivated by advances in both single-molecule spectroscopy and nanoscale fabrication. First, single-molecule spectroscopy provides the possibility of verifying the theoretical models in great detail, and has led, for example, to the observation of a continuous transition from photoluminescence (PL) enhancement to quenching[5] and to the observation of an excited-state lifetime reduction simultaneous with a PL enhancement.[6,7] Second, nanoscale fabrication offers the possibility of engineering plasmonic structures with high precision. This is of crucial importance because fluorescence enhancement and quenching depend differently on nanostructure properties such as material, size, and shape, as well as on emitter−nanostructure separation distance.[3,4] Only in a limited part of this extensive parameter space can plasmonic nanostructures provide substantial improvements to the radiative properties of emitters.[8]

Apart from influencing the balance between fluorescence enhancement and quenching, the nanostructure geometry also affects the polarization and directionality of the enhanced fluorescence.[9] Experimental evidence of the influence of metallic nanostructures on PL polarization has been attained with single quantum-dot measurements on rough metal surfaces.[10]

In this letter, we report on the enhancement of Si QD PL upon coupling the Si QDs to elongated Ag nanoparticles.[11] The observed polarization selectivity enables us to conclude that, under the present excitation conditions, the PL enhancement is due to the coupling of the silicon quantum-dot emission dipoles with dipolar plasmon modes in the Ag nanoparticles, rather than due to an enhancement of the excitation rate. This conclusion follows directly from the correspondence between the measured PL and extinction data, and it does not rely on, for example, a rate-equation model. A compelling property of Si QDs that is utilized in this study is their broad emission spectra, which enables the identification of spectral trends in PL enhancement over a wide wavelength range upon varying the nanoparticle properties.[12]

Si QDs were produced by ion implantation of 11-keV Si^+ ions to a fluence of 1.7×10^{16} cm^{-2} into a 1.0-mm-thick

* Corresponding author. E-mail: mertens@amolf.nl.
† Center for Nanophotonics, FOM Institute for Atomic and Molecular Physics.
‡ California Institute of Technology.

10.1021/nl061494m CCC: $33.50
Published on Web 10/24/2006

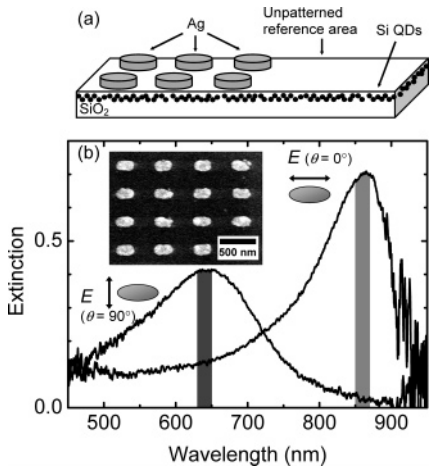

Figure 1. (a) Schematic representation of the sample consisting of an SiO_2 substrate, which is doped with Si quantum dots at a depth of about 10 nm, with an array of elongated Ag nanoparticles on top. (b) Extinction spectrum of an array of elongated Ag nanoparticles for two polarizations: parallel and perpendicular to the long axis (both measured at normal incidence). The bars centered at 640 and 860 nm indicate the wavelength ranges that are considered in Figure 2, as well as in Figure 3b and c. Inset: Scanning electron micrograph of the same array.

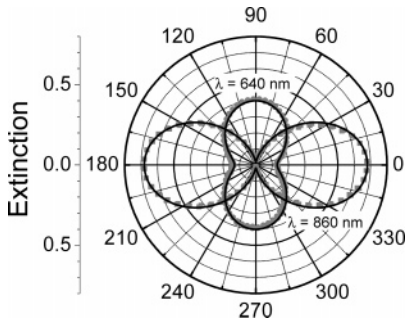

Figure 2. Polar plot of the extinction as a function of the polarization angle θ relative to the nanoparticle long axis measured on an array of elongated Ag nanoparticles for two wavelengths: 640 and 860 nm (symbols). The solid lines are fits to the experimental data by dipole patterns (see the text).

silica substrate (suprasil, Hereaus). Monte Carlo simulations performed with SRIM (ref 13) indicate that such an implantation yields a Gaussian depth distribution of Si in the SiO_2, with a peak excess Si concentration of 10% at a depth of ~20 nm. The implanted silica was annealed in Ar for 20 min each at 200 °C and 450 °C, and then for 30 min at 1000 °C, to form Si QDs with typical diameters of 2−5 nm.[14] The samples were subsequently heated in forming gas (10% H_2, 90% N_2) for 30 min at 450 °C to passivate defects. After Si QD formation, the QD distribution was brought to an average depth of about 10 nm from the surface by etching the oxide in 2.3% HF(aq). The etch rate was 0.25 nm/s, as determined by spectroscopic ellipsometry on an analogous sample of SiO_2 on a Si substrate. Ellipsometry also indicated that after etching the surface roughness was less than 0.2 nm.

On top of the Si-QD-doped SiO_2 substrates, elongated Ag nanoparticles were fabricated using electron-beam lithography. Silver was chosen because this metal exhibits the lowest Ohmic damping at visible and infrared frequencies, and thus gives rise to the highest electromagnetic field enhancements. First, the surface of the QD-doped SiO_2 was cleaned in a 5:1:1 $H_2O/H_2O_2/NH_4OH$ solution. Subsequently, an electron-beam lithography system was used to pattern a $50 \times 50\ \mu m^2$ array of elongated ovals (with typical dimensions of ~100 nm and at a pitch of ~400 nm) on a spin-coated dual layer of polymethylmethacrylate (PMMA) covered by a 17 nm Ge conduction layer. After removing the Ge and developing the resist, a 2 nm Si wetting layer and a 20 nm Ag layer were deposited onto the structure by electron-beam evaporation under ultrahigh vacuum conditions. The remaining PMMA was lifted off, leaving an array of elongated Ag nanoparticles on the substrate. The resulting structure is sketched in Figure 1a, and a scanning electron micrograph (SEM) image of the array is displayed as an inset in Figure 1b. The dimensions of these nanoparticles are: $240 \times 140 \times 20\ nm^3$.

Because of the anisotropic particle dimensions, the fabricated Ag nanoparticle array exhibits polarization-dependent extinction spectra, as is shown in Figure 1b. These extinction spectra were measured in an optical microscope by white-light illumination through a 60x objective (NA = 0.8) from the top, and collection through a 20x objective (NA = 0.4) from the bottom, after which the light was passed through a polarizer. The plotted extinction, E, is defined as $E = 1 - T$, where T is the intensity transmitted through the array relative to the intensity transmitted through the unpatterned reference area. Therefore, the extinction is a measure of the fraction of light that is removed from the forward-propagating beam by absorption and scattering due to the nanoparticles. Figure 1b shows extinction spectra measured on one particular array for two polarizations angles θ: parallel ($\theta = 0°$) and perpendicular ($\theta = 90°$) to the long axis. For both polarizations, a pronounced peak in extinction can be observed. These relatively broad features can be associated with the excitation of plasmon modes in the Ag nanoparticles.[15] The extinction spectrum for $\theta = 90°$ exhibits a peak at 640 nm, whereas the extinction for $\theta = 0°$ reaches its maximum around 860 nm. Because of reduced white-light intensity as well as reduced detector sensitivity, the extinction spectra are less accurate above 900 nm. The polarization dependence of the extinction can be understood qualitatively based on the fact that the nanoparticle surface charge distributions generated by plane-wave illumination are different for the two polarizations. Accordingly, dissimilar restoring forces are built up, which leads to blue- and red-shifted resonance frequencies for transverse and longitudinal polarizations, respectively. The extinction spectra do not exhibit features that indicate a diffractive response of the nanoparticle array,[16−18] which implies that, for the present geometry, interparticle coupling is relatively weak.

Figure 2 shows a polar plot of the extinction as function of the polarization angle θ for two characteristic wavelengths: 640 and 860 nm. The data exhibit dipole-like polarization patterns that are oriented perpendicular to one another. In fact, the measured extinction data for 860 nm can be fitted perfectly by a dipole pattern: $E = A \cos^2 \theta$, with $A = 0.68$ (solid line), where 0.68 corresponds to the

extinction at 860 nm measured at $\theta = 0°$, as shown in Figure 1b. The polar plot of the extinction at 640 nm can be fitted very well by a superposition of two dipolar patterns that are oriented perpendicular with respect to each other: $E = B \sin^2\theta + C \cos^2\theta$, with $B = 0.40$ and $C = 0.14$ (solid line). These numbers are in agreement with the extinction values at 640 nm for the two spectra shown in Figure 1b; the second term thus represents the tail of the longitudinal extinction feature. The good agreement between the experimental data and the fits shows that the extinction is dominated by the dipolar plasmon modes of the Ag nanoparticles. The fact that higher-order multipole modes do not need to be invoked is attributed to the small dimensions of the nanoparticles compared to the wavelength of light.

On the same array for which the extinction was measured, PL spectra were acquired under excitation from a frequency-doubled Nd:YAG laser operating at an excitation wavelength of $\lambda_{exc} = 532$ nm that was focused onto the sample surface through a microscope objective (see Figure 1a) to a 10-μm-diameter spot (corresponding to an area containing ~500 nanoparticles). A relatively high pump power, 10^4 W/cm^2, was used to ensure operation near the saturated pump-power regime, where the PL intensity is limited by the radiative decay rate and is independent of the internal quantum efficiency. The polarization of the pump source was kept constant during all measurements. The PL intensity was collected from the bottom, passed through a polarization analyzer, and subsequently recorded using a thermoelectrically cooled CCD detector in conjunction with a 30-cm-focal-length grating spectrograph. A dichroic filter that absorbs light below 550 nm was used to eliminate incident laser light from the detector.

Figure 3a shows PL spectra measured on the unpatterned reference area and on the nanoparticle array, the latter for two polarization angles: $\theta = 0°$ and $\theta = 90°$. The reference spectrum is a typical ensemble-averaged Si QD PL spectrum that spans a relatively wide wavelength range (~600−1000 nm), which is due to both homogeneous and inhomogeneous broadening. The PL intensity on the array is found to be enhanced in a strongly wavelength- and polarization-dependent way compared to the reference. The maximum enhancements at the emission wavelengths of $\lambda_{em} = 640$ nm and $\lambda_{em} = 860$ nm, for $\theta = 90°$ and $\theta = 0°$ respectively, exceed a factor of 3. Such enhancement values can be observed by collecting through the substrate as well as from the top side.[12] These numbers represent ensemble-averaged values, and much larger enhancements are expected at lightning-rod-type hotspots close to the sharp corners of the Ag nanoparticles.

To enable a more detailed analysis of the polarization dependence of the PL enhancement, Figure 3b and c displays polar plots of the PL intensity as function of the polarization angle of the emission measured both on the array and on the unpatterned reference area for $\lambda_{em} = 640$ nm and $\lambda_{em} = 860$ nm, respectively. For both wavelengths, the PL intensity on the reference area (circular line in the center of each plot) is polarized isotropically, so the data are not dependent on the polarization of the pump light. Indeed, the absence of polarization memory has also been observed for single Si QDs.[19] Furthermore, any orientation dependent emission due to a small size anisotropy for single Si QDs[19] is expected to be averaged out for Si QD ensembles in an amorphous SiO_2 matrix.

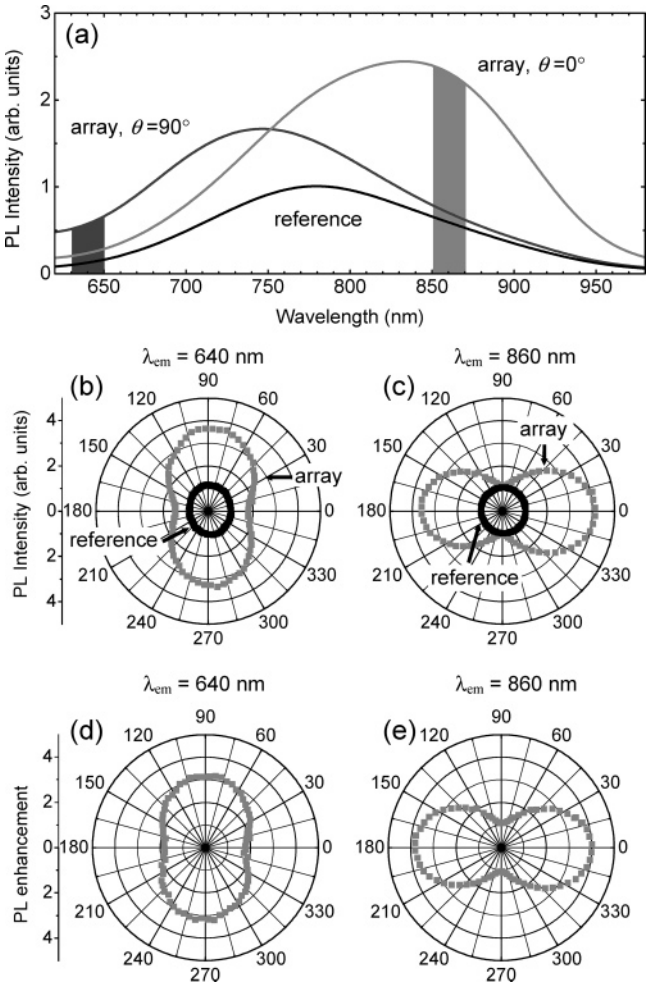

Figure 3. (a) Si quantum-dot photoluminescence spectra measured on the reference area and on the array, the latter for two emission polarization angles θ (relative to the nanoparticle long axis): $\theta = 0°$ and $\theta = 90°$. The bars indicate the wavelength ranges that are considered in parts b and c. (b) Polar plot of the Si QD photoluminescence as function of θ for $\lambda_{em} = 640$ nm. (c) Data similar to that in part b for $\lambda_{em} = 860$ nm. (d) Polar plot of the Si QD photoluminescence enhancement as function of θ for $\lambda_{em} = 640$ nm. (e) Data similar to that in part d for $\lambda_{em} = 860$ nm. Pump wavelength: 532 nm.

As can be seen in Figure 3b and c, the PL intensity on the array is enhanced compared to the reference. Moreover, this enhancement is polarized in the same direction as the extinction at the emission wavelength, for both $\lambda_{em} = 640$ and $\lambda_{em} = 860$ nm (cf. Figure 2). Note that these perpendicularly oriented PL enhancement patterns, including the supporting extinction data, were obtained from a single array of elongated Ag nanoparticles. Besides, the PL measurements were done without changing the polarization of the pump light, so the excitation conditions for the array measurements at $\lambda_{em} = 640$ and $\lambda_{em} = 860$ nm were completely identical. Consequently, the striking correspondence between the polarization dependence of the extinction at the emission wavelength on one hand, which can be associated with

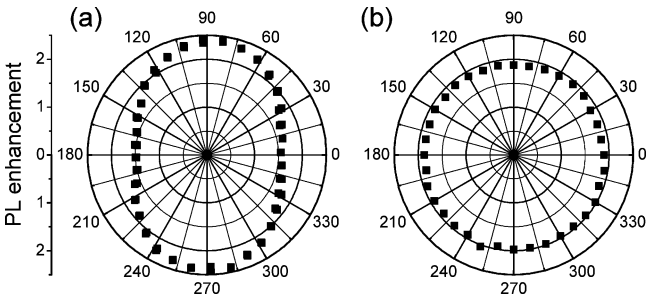

Figure 4. Polar plots of the Si QD photoluminescence intensity versus the polarization angle of (a) the emission and (b) the pump light, both with respect to the long axis of the nanoparticles. Emission wavelength, 790 nm; pump wavelength, 532 nm.

dipolar plasmon modes, and the polarization dependence of the PL enhancement on the other hand shows that the PL enhancement is due to the electromagnetic coupling of the Si QD emission dipoles with dipolar plasmon modes of the Ag nanoparticles.

It can be noted that the profiles in Figure 3b and c are not completely symmetric for rotation over 180°. For example, the PL intensity on the array is higher at $\theta = 0°$ than at $\theta = 180°$ in Figure 3c. This asymmetry is attributed to a small misalignment in our setup. Indeed, by normalizing the angular profiles of the arrays by the reference data, perfectly symmetric curves are observed, is seen in Figure 3d and e.

The correspondence between the polarization dependences of the PL enhancement on one hand and the extinction at the emission wavelength on the other hand strongly suggests that the observed PL enhancement is not caused by a plasmon-induced enhancement of the Si QD excitation rate. In particular, at the emission wavelength of 860 nm, the emission polarized perpendicular to the long axis ($\theta = 90°$) is hardly enhanced (see Figure 3c). This is attributed to the fact that at 860 nm there is practically no spectral overlap with plasmon modes, for $\theta = 90°$ (see Figure 1), so there can be no resonant coupling of the Si QD emission dipoles with the plasmon modes at this wavelength. However, if the observed PL enhancement would be partially caused by an enhanced excitation rate, then the enhancement shown in Figure 3c should contain an emission-polarization-independent contribution, which would be present at $\theta = 90°$ as well. The fact that such a contribution is not observed indicates that the PL enhancement is not caused by a plasmon-induced enhancement of the excitation rate.

In order to verify this hypothesis more explicitly, we performed a control experiment in which we measured the PL enhancement as function of pump polarization. Ag nanoparticle arrays with a slightly smaller aspect ratio than those in Figure 3 and covered with a 20-nm-thick Si layer were used. As shown in Figure 4a, these samples also exhibit polarized emission, at their resonance wavelength of 790 nm (measured for a fixed pump polarization). The polarized emission is indicative of the anisotropic plasmonic properties of the Ag nanoparticles. Figure 4b displays a polar plot of the PL enhancement versus polarization angle of the pump light (measured without polarization filtering of the emission). This graph shows a completely isotropic response, and therefore it can be concluded that the observed PL enhancement is not caused by a plasmon-induced enhancement of the Si QD excitation rate.

In conclusion, we have observed a polarization-selective PL intensity enhancement upon coupling Si QDs to engineered elongated Ag nanoparticles. The dependences of the PL enhancement on pump and emission polarization show unambiguously that the PL enhancement is due to the electromagnetic coupling of the Si QD emission dipoles with dipolar plasmon modes in the Ag nanoparticles. The polarization selectivity enables us to draw this conclusion without relying on, for example, rate-equation models. The measured ensemble-averaged PL enhancements exceed a factor 3, and much larger enhancement values are expected close to the sharp corners of the metal nanoparticles. The observed polarization selectivity demonstrates that plasmonic nanostructures enable the optimization of light sources not only by enhancing emission rates but also by affecting the polarization of the enhanced emission.

Acknowledgment. We thank Kobus Kuipers for fruitful discussions. This work is part of the research program of the "Stichting voor Fundamenteel Onderzoek der Materie (FOM)", which is financially supported by the "Nederlandse organisatie voor Wetenschappelijk Onderzoek (NWO)". This work was also partially supported by NANONED, a nanotechnology program of the Dutch Ministry of Economic Affairs, by NSF Grant No. CHE-0213589, and by AFOSR MURI Award Nos. FA9550-05-1-0450 and FA9550-04-1-0434.

References

(1) Moskovits, M. *Rev. Mod. Phys.* **1985**, *57*, 783.
(2) Wokaun, A.; Lutz, H.-P.; King, A. P.; Wild, U. P.; Ernst, R. R. *J. Chem. Phys.* **1983**, *79*, 509.
(3) Gersten, J.; Nitzan, A. *J. Chem. Phys.* **1981**, *75*, 1139.
(4) Wokaun, A.; Gordon, J. P.; Liao, P. F. *Phys. Rev. Lett.* **1982**, *48*, 957.
(5) Anger, P.; Bharadwaj, P.; Novotny, L. *Phys. Rev. Lett.* **2006**, *96*, 113002.
(6) Farahani, J. N.; Pohl, D. W.; Eisler, H.-J.; Hecht, B. *Phys. Rev. Lett.* **2005**, *95*, 17402.
(7) Kühn, S.; Håkanson, U.; Rogobete, L.; Sandoghdar, V. *Phys. Rev. Lett.* **2006**, *97*, 017402.
(8) Mühlschlegel, P.; Eisler, H.-J.; Martin, O. J. F.; Hecht, B.; Pohl, D. W. *Science* **2005**, *308*, 1607.
(9) Blanco, L. A.; García de Abajo, F. J. *Phys. Rev. B* **2004**, *69*, 205414.
(10) Shimizu, K. T.; Woo, W. K.; Fisher, B. R.; Eisler, H. J.; Bawendi, M. G. *Phys. Rev. Lett.* **2002**, *89*, 117401.
(11) Ditlbacher, H.; Felidj, N.; Krenn, J. R.; Lamprecht, B.; Leitner, A.; Aussenegg, F. R. *Appl. Phys. B* **2001**, *73*, 373.
(12) Biteen, J. S.; Lewis, N. S.; Atwater, H. A.; Mertens, H.; Polman, A. *Appl. Phys. Lett.* **2006**, *88*, 131109.
(13) Ziegler, J. F.; Biersack, J. P.; Littmark, U. *The Stopping and Range of Ions in Solids*; Pergamon: New York, 1985.
(14) Brongersma, M. L.; Polman, A.; Min, K. S.; Boer, E.; Tambo, T.; Atwater, H. A. *Appl. Phys. Lett.* **1998**, *72*, 2577.
(15) Kreibig, U.; Vollmer, M. *Optical Properties of Metal Clusters*; Springer: Berlin, 1995.
(16) Zou, S.; Schatz, G. C. *J. Chem. Phys.* **2004**, *121*, 12606.
(17) Hicks, E. M.; Zou, S. S.; Schatz, G.; Spears, K.; Van Duyne, R.; Gunnarsson, L.; Rindzevicius, T.; Kasemo, B.; Käll, M. *Nano Lett.* **2005**, *5*, 1065.
(18) Félidj, N.; Laurent, G.; Aubard, J.; Lévi, G.; Hohenau, A.; Krenn, J. R.; Aussenegg, F. R. *J. Chem. Phys.* **2005**, *123*, 221103.
(19) Valenta, J.; Juhasz, R.; Linnros, J. *Appl. Phys. Lett.* **2002**, *80*, 1070.

NL061494M